DOI:
10.1039/C9TB02582K

Document Version
Peer reviewed version

Journal Name

ARTICLE

Conjugated polymers as nanoparticle probes for fluorescence and photoacoustic imaging

Received 00th January 20xx,
Accepted 00th January 20xx

DOI: 10.1039/x0xx00000x

www.rsc.org/

Thais Fedatto Abelha [a], Cécile A. Dreiss [a], Mark A. Green *[b], Lea Ann Dailey*[c]

Bioimaging enables the visualisation of biological processes at the microscopic and macroscopic levels, finding applications from cellular tracking to whole body scanning for diagnosis purposes. The different techniques developed to acquire images make use of most radiation types of the electromagnetic spectrum. Recently, there has been interest in non-ionising radiation imaging techniques that can offer improved detection or additional information about biological processes, and fluorescence and photoacoustic imaging have become an eminent field. Conjugated polymers are versatile materials for bioimaging due to their tailored absorption and emission spectra and applications in both fluorescence and photoacoustic imaging. This review gives an overview on bioimaging techniques, with a special focus on conjugated polymer nanoparticles (CPNs), the different types of nanoparticle chemistries published and their preclinical safety assessment.

Introduction

Conjugated polymers are versatile materials that have been employed in light emitting devices [1], solar cells [2] and as contrast agents for bioimaging [3–6]. The large scope of applications in different fields is related to their many useful properties, which include charge carrier transport [7], tuneable optical properties [8] and bright fluorescence with good photostability [9]. They are also highly processable, allowing the efficient manufacture of solar cells [2], and flexible light emitting displays [1,10]. They can also be engineered into electromechanically active devices [11] and can form nanoparticles with diverse biomedical applications [12,13]. The fact that they are organic materials has also boosted the interest in their biological application, which has been evidenced in the recent efforts to produce biodegradable conjugated polymers [14,15]. Besides being used for bioimaging, CPNs have also been studied as drug delivery systems [12], including photoresponsive drug release [16], biosensors [17] and as theranostic agents for cancer treatments [18–20]. In this review, we discuss the role of conjugated polymers in the bioimaging field, focusing on their formulation into nanoparticles and their early safety screening.

Bioimaging

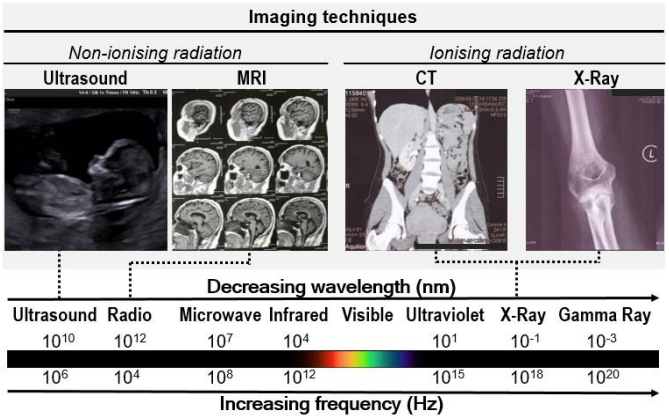

Figure 1: A representation of the electromagnetic spectrum (bottom) and common clinical imaging techniques that use ionising and non-ionising radiation (top). Computed tomography (CT) and magnetic resonance imaging (MRI). Reproduced from Abelha (2018) [21].

Biomedical imaging encompasses a wide range of non-invasive imaging modalities that generate anatomical and physiological information. The different techniques developed to acquire images make use of most radiation types of the electromagnetic spectrum (Figure 1) [22]. Radiation is composed of photons, which show a particle/wave-like behaviour and can carry different amounts of energy [23]. Each photon's energy is directly proportional to its frequency and inversely related to its wavelength [24]. Below 200 nm, a photon has sufficient energy to cause ionisation [25], a process in which an electron bound to an atom is removed [24]. This process is caused by matter absorption of radiation at high frequency and very short wavelengths, such as gamma-rays, X-rays [24] and the ultraviolet (UV) radiation [26,27]. Above the UV region, the non-ionising visible region of the electromagnetic spectrum [28] is composed of wavelengths in the range of 400-700 nm [29], which is followed by the

[a] King's College London, Institute of Pharmaceutical Science, 150 Stamford Street, SE1 9NH, London, UK.
[b] King's College London, Department of Physics, Strand Campus, WC2R 2LS, London, UK. Email: mark.a.green@kcl.ac.uk
[c] University of Vienna, Institute of Pharmacy, Vienna, Austria. Email: leaann.dailey@univie.ac.at

† Footnotes relating to the title and/or authors should appear here.
Electronic Supplementary Information (ESI) available: [details of any supplementary information available should be included here]. See DOI: 10.1039/x0xx00000x

spectral regions of decreasing energy classified as infrared, microwave, radio and ultrasound waves [30].

Established bioimaging techniques

Visible-light microscopy is a well-established optical imaging technique broadly used for research and clinical diagnosis [31,32]. Colourful materials and fluorescent dyes have been broadly used to enhance microscopic structures, enabling the visualisation of tissue architecture and of relevant biological processes with high specificity [31]. Fluorescent biological labels have also been used in immunohistochemistry to detect specific macromolecules in tissues and cells, such as cellular receptors involved in cancer [33,34]. In addition to the clinical and research relevance of microscopy-based analysis, fluorescent immunoconjugates, nucleic acid stains and physiological probes are also largely used in flow cytometry to characterise different cell populations, their viability and physiological processes [35–37]. Overall, the non-ionising visible spectral region is used for fluorescence imaging at microscopic level and the use of specific wavelengths enables the assessment of different parameters simultaneously in live cells, *ex vivo* or in fixed tissues [37,38].

The techniques currently used for body imaging are based on the exposure to ionising or non-ionising electromagnetic radiation [22]. In spite of the restrictions of patient exposure to ionising radiation, nuclear imaging techniques are the standard modality for clinical use due to the high tissue penetration and sensitivity [22,39]. Among the different ionizing techniques, X-ray computed tomography (CT) is a well-established and largely used diagnostic tool that currently enables high resolution with the use of contrast agents for soft tissue imaging [40]. The CT technique has been used since 1972 and is based on the tendency of materials of high density and atomic number to absorb X-ray radiation [40]. As a replacement or combined with CT, positron emission tomography (PET) is used to track specific molecular targets by measuring gamma-rays emitted from inside the body following administration of positron-emitting isotopes [41].

In the past 30 years, magnetic resonance imaging (MRI) emerged as a powerful and high resolution non-ionising technology [42,43]. MRI is based on the detection of radiowaves emitted by hydrogen atoms present in the body and/or administered contrast agents (e.g. gadolinium or iron oxide) under a powerful magnetic field [43,44]. Another non-ionising technique commonly used is ultrasound (also referred to as sonography), which has been used since the post-World War II period [45,46]. Upon the incidence of an ultrasound beam, a visual image is created from the reflection of ultrasonic echoes by tissues with different acoustic impedance [46]. In general, a denser and more solid structure will reflect more ultrasound waves, which are visualised as a white area, while a fluid transmits most of the waves and, due to the lower reflection, produces darkened areas in ultrasound images [47].

Emerging bioimaging techniques

Recently, there has been great interest in *in vivo* imaging techniques that can offer improved detection or additional information about biological processes and, among different approaches, optical imaging has become prominent [48,49]. The light emission of endogenous compounds following exposure to radiation (known as auto-fluorescence) has been exploited for research and medical diagnostics [50–52] and fluorescent contrast agents are also used in guided surgery for cancer [53]. While localized fluorescence imaging is used in the clinic, the whole body imaging in the optical region of the spectra is currently applicable to small animals [48,54]. Whole body fluorescence imaging typically makes use of regions of the electromagnetic spectra that present lower interference from tissue optical properties [22]. In the UV and visible regions, the biological tissues can promote significant light scattering, absorbance and emission [51]; however, above the near infrared (> 700 nm), these effects are less dominant and allow increased radiation penetration [55]. Although fluorescent contrast agents present high sensitivity and can be used in picomolar concentrations, optical imaging is restricted by the body's attenuation of light and sufficient tissue penetration is only achieved in the near infrared region of the spectra [56]. Indocyanine green, which has an excitation range of 760-785 nm and fluorescence emission between 820-840 nm, is the most studied near infrared fluorescent dye, primarily because it is a FDA (USA Food and Drug Administration agency) approved material [39,57]. For example, near infrared imaging with indocyanine green enabled image acquisition of the lymphatic system architecture in the limbs of healthy volunteers and patients with lymphedema (disruption of lymph transport) [58]. Although indocyanine green has shown success in clinical use, near-infrared imaging is restricted to 3-4 cm penetration depth [59] , accordingly, there remains a large scope for improvement in the development of near infrared imaging contrast agents, particularly with regards to new fluorescent dyes and nanoparticle based systems [60].

Another emerging imaging technique that also involves the optical region of the electromagnetic spectrum is photoacoustic imaging [3,5,18,61–64]. This promising technique relies on the photoacoustic effect, which can be defined as the production of sound by light [65] and is based on the conversion of light absorbance energy into heat, which leads to tissue thermal expansion and results in the emission of ultrasound waves [63,66]. The increasing interest in photoacoustic imaging is due to the lower scattering of acoustic waves in comparison with photons, which has enabled imaging at increased depths and with improved resolution compared to imaging techniques that purely rely on the optical spectral region [3,64,67]. Similar to ultrasound imaging, photoacoustic imaging also detects ultrasound waves, but the difference between the two techniques is that the former is only based on sound, whereas the latter makes use of laser light as an irradiation source [61]. The image acquisition by photoacoustic imaging takes advantage of the variable tissue distribution of endogenous light absorbing components, such as haemoglobin, collagen, lipids and water, and their particular light absorbance characteristics [63]. Accordingly, the technique can distinguish anatomical features while also providing physiological information (e.g. tissue oxygenation or anaemia) [61,63]. In this context,

optoacoustic tomography of the human breast generated high resolution images with 1 cm penetration depth, which enabled the distinction between patients diagnosed with breast carcinoma and healthy volunteers [68]. Notably, the imaging of breast tissue has the potential to achieve 10 cm penetration depth, if opposite sides of the tissue are illuminated; however optoacoustic imaging is generally restricted to 5-7 cm penetration depth [69].

In addition to naturally occurring chromophores, exogenous near infrared contrast agents can be used to generate a high contrast image with deep tissue penetration [4,5,61]. Contrast agents composed of a variety of materials have been developed and many are conjugated with relevant biomarkers for targeted detection of disease, especially cancer [63]. For example, CPNs with broad near-infrared absorbance functionalised with folate for targeted breast cancer imaging generated a good contrast image in a mouse model [5]. Similar approaches were performed using gold nanorods as a contrast agent for targeted prostate cancer detection [66] and single-walled carbon nanotubes conjugated with peptides could also be seen to accumulate in tumours and enhance tumour detection [67]. Further examples include non-functionalised nanoparticles containing the photoacoustically active derivative of perylene-3,4,9,10-tetracarboxylic diimide, which was detected in murine brain tumours following injection into the brain [70], and CPNs that showed strong fluorescence and photoacoustic signal, enabling lymph node imaging following intravenous administration in mice [3].

The bioimaging techniques currently available present different limitations with regards to their sensitivity, resolution and penetration depth [71]. Consequently, diverse nanomaterials have been explored to address these issues in an attempt to improve the performance of imaging procedures [71]. Among the different types of materials investigated as new fluorescent imaging agents, there has been an interest in alternative fluorophores, such as inorganic quantum dots [72] and π-conjugated polymers [60]. CPNs are attractive candidates for cellular labelling and biomedical imaging due to their tailored absorption and emission spectra and amenable use both for fluorescence and photoacoustic imaging [5]. In addition, nanoparticles often present the advantage of being brighter, more photostable and easily designed for targeted delivery compared to small molecule dyes [60].

CPNs as bioimaging contrast agents

The field of conjugated polymers has its origin as early as 1862, with the synthesis of a partly conductive material by H. Letheby of the College of London Hospital [73]. However, it was only after 1977 that the area witnessed a remarkable growth due to the study of the first conjugated polymer, polyacetylene [7,74]. This breakthrough led to the development of innovative materials and their importance was recognised by the award of the 2000 Nobel prize in chemistry to Alan Heeger, Alan MacDiarmid and Hideki Shirakawa [73,75]. Particularly, the development of the second generation of conjugated polymers, which are more soluble and processable materials, has allowed the use of such materials in electroluminescent devices, a property that was first reported in 1990 in a study of PPV [76]. As a consequence, different conjugated polymers have been investigated as light sources in various devices, such as light-emitting diodes (LEDs) [8,75]. A further field of applications emerged in 1999 when Chen *et al*. reported on the development of a highly sensitive fluorescent biosensor using conjugated polymers [77,78].

One feature that characterises conjugated polymers is the presence of alternating double bonds [7]. The successive distribution of carbons with π-bonding allows the π-electron orbitals to overlap, leading to an electron delocalization along the polymer backbone chain, and, as a result, the electrons are able to move freely [7,79,80]. Excitations within the π-band generate π-π* transitions with a particular energy gap (defined by the chemical structure) that account for the useful photo-conductive properties of conjugated polymers [81]. However, electron delocalisation alone doesn't allow a conjugated polymer to conduct electricity and, usually, charge carriers (dopants) are needed in order to alter its electrical properties [73]. Dopants can either donate electrons to or remove them from the chemical structure, increasing the number of free charges, which can be moved by an external applied voltage [8,73,81]. Most importantly, conjugated polymers can be used for different applications both in undoped and doped states [80].

Many conjugated polymers show strong photoluminescence in the visible and near infrared spectrum in their natural undoped state and doping allows researchers to tune the optical properties [82]. Also, as the colour of the emitted light is defined by the band gap of the π-π* electronic transition, any structural change will have an effect on the emitted region of the spectra [8] (**Figure 2**). In this context, attempts to control the energy gap and, therefore the properties of conjugated polymers, rely mainly on doping the material and also on refining its chemical structure [12,81,83–85].

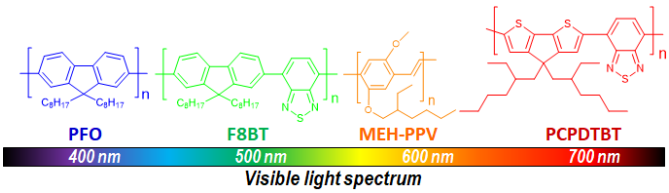

Figure 2: Conjugated polymers with various chemical structures and their corresponding emission regions in the visible light spectrum.

Conjugated polymers have emerged as excellent materials for making fluorescent nanoparticles [86–88] and they can exhibit high quantum yields depending on their chemical structure and degree of polymerisation [89,90]. CPNs showed good properties for *in vivo* fluorescence imaging in mice [85,91] and for cell labelling of different cell lines [9,87,92–99] (**Figure 3**), showing good cytocompatibility [12,15,88,97]. Furthermore, near infrared absorbing CPNs exhibited excellent contrast properties for *in vivo* photoacoustic imaging of cancer in mice [3,5,100]. In addition to their role as photoacoustic probes, CPNs have also been investigated for their potential as theranostic agents, (e.g. for tumour ablation) [18] and as drug delivery systems for chemotherapeutics [12,16]. Due to their promising performance in the proof of concept studies mentioned above, recent interest has been focused on the development of biodegradable conjugated polymers

[14], which are more likely to be eliminated following *in vivo* administration, facilitating their future clinical application.

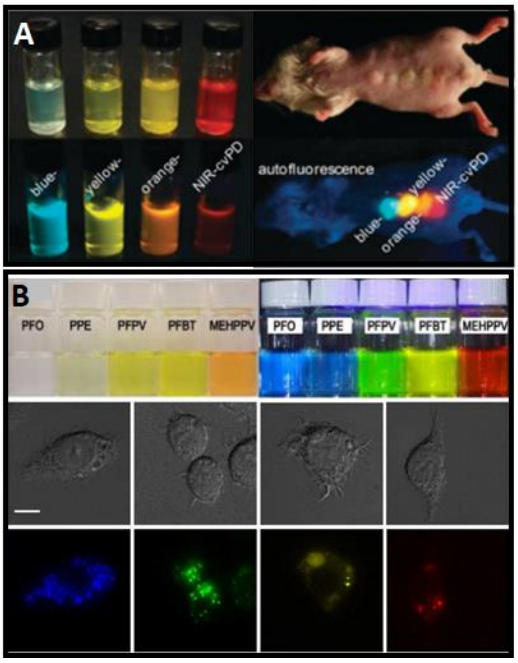

Figure 3: CPNs under ambient light and UV illumination of substituted derivatives of poly(p-phenylenevinylene) with tailored optical properties according to their side chain structure (A) and of conjugated polymers of varied chemical structures (B). The CPNs acting as fluorescent probes *in vivo* (A) and staining mice macrophages *in vitro* (B). Reproduced from Ref. [85] (A) Kim, S. et al (2010), Chemical Communications, 46(10), 1617–19 with permission from The Royal Society of Chemistry. Reprinted with permission from C. Wu, B. Bull, C. Szymanski, K. Christensen and J. McNeill (B) [9]. Multicolor Conjugated Polymer Dots for Biological Fluorescence Imaging. *ACS Nano*, 2008, **2**, 2415–2423. Copyright 2008 American Chemical Society.

Nanoparticles as carriers of conjugated polymers

Nanoparticle properties

Nanomaterials can be defined as particles with nanoscale dimensions (one dimension must be below 1000 nm) [101,102] or, according to a more restrictive definition, as particles with dimensions in the range of 1-100 nm that present distinct properties in comparison to the same material with larger sizes [103,104]. Nanoparticles designed for biomedical applications can be found in the full nanoscale size range; however, in practice, nanoparticles with diameters of 5-250 nm typically present useful properties [105]. Nanoparticles have gained increased research interest, because they can be designed for targeted delivery, for instance with built-in pH-responsive systems [106] or antibody conjugation [107], and they show increased circulation time and reduced toxic effect in comparison to their corresponding free-compounds [108]. Moreover, nanoparticles present increased cellular uptake and accumulate in cancerous areas or inflammatory sites due to the enhanced permeability and retention (EPR) effect [108–111].

First described in 1986, the EPR effect was related to the leaky hypervasculature of tumour areas, resulting in the accumulation of circulating macromolecules [109]. The permeable capillaries present in tumour areas present a porous structure that varies from tumour type and animal species [112–114]. In mice, the passive accumulation of liposomes due to EPR effect revealed a cut-off size of 400-600 nm [113] and of 380-780 nm and 1.2-2 μm [112] depending on the tumour type. The EPR process can take 6-24 hours [115,116] and enhanced contrast for imaging of tumours has been reported after 24 and 48 hours for fluorescent materials [116]. However, the EPR effect is heterogeneous amongst patients and tumour types and, although nanoparticles have been widely studied for the diagnosis and treatment of cancer, different tumour characteristics limit the usefulness of the EPR effects in clinical applications [117]. In this context, it is relevant to mention that the passive CPN accumulation in the tumour due to EPR effect was shown to lead to lower contrast than targeted CPNs [5].

The nanoparticle shape, size, chemical composition and surface properties play an important role in its cellular uptake, clearance and biodistribution [110,118]. After administration, nanoparticles encounter a complex environment rich in biomacromolecules, which can interact with the particle surface, forming a protein corona due to adsorption [119,120]. Protein adsorption is dependent on the nanoparticle size and surface properties (charge and chemical composition); [121] in general, nanoparticles with a neutral surface charge have shown lower protein adsorption in comparison to cationic and anionic systems [121]. They also exhibited increased circulation times and lower non-specific cellular uptake [122]. The protein corona influences the fate of the nanoparticles, as they can be rapidly removed from blood circulation due to recognition and interaction with phagocytic immune cells in a process named opsonisation, which often take place in organs with high blood flow such as liver and spleen [105,122,123].

Once in circulation, nanoparticles are subjected to a size-dependent clearance related to the morphological features of the blood capillaries endothelia, which are classified as continuous, fenestrated or discontinuous [122]. A continuous capillary has a tight structure, while fenestrated and discontinuous capillaries are more leaky to macromolecules [124]. Different organs contain a particular type of capillary, with the continuous structure being the most abundant [105], and the pore can vary in size and number between mammal species [124,125]. In general, the kidney capillaries have a fenestrated structure with pore sizes of *ca.* 15 nm, while discontinuous capillaries in the liver have larger gaps of 50-180 nm and in the spleen they may be up to 5 μm [124]. As a consequence, nanoparticles and macromolecules with diameters smaller than 5 nm are rapidly excreted through renal clearance [126], while larger structures can accumulate in the liver and spleen [105,110].

Nanoprobes of conjugated polymers

Conjugated polymers have been formulated into different nanostructures, not only to explore the advantages of a nanoparticle

delivery system, but also because they generally are hydrophobic materials that need to be dispersed in an aqueous vehicle for biological applications [127]. To stabilise the formation of nanoparticles containing hydrophobic conjugated polymers, PEGylated excipients are often used [5,18,60,87,91]. Linking PEG to biomedical molecules has been widely explored because it brings many advantages, such as enhancing drug solubility, decreasing immunogenicity, prolonging residence in the body and decreasing degradation by metabolic enzymes [111]. PEG creates a steric stabilisation effect by forming a hydrophilic layer on the surface of nanoparticles that prevents the interaction with blood components, which is also referred to as a stealth behaviour [128]. As consequence, PEGylation changes the physicochemical properties of biomedical molecules, resulting in improvements in their pharmacokinetic behaviour [129].

CPNs can be constituted solely of conjugated polymers [6,12] or of conjugated polymers linked to PEG, which self-assemble into nanoparticles due to their inherent amphiphilicity [14,130]. Alternatively, hydrophobic conjugated polymers can be encapsulated within a nanoparticle matrix [18,88,92,94,97,131,132]. Besides facilitating the formation of nanoparticles and ensure their colloidal stability, coating agents may also be used to provide a neutral charge to CPNs [133] and to enable bioconjugation with targeting molecules [92,133]. Overall, CPNs have been prepared with varied material composition, which includes lipids [3,19,88,93,134] proteins [100,135], polymers [94,132,136] and surfactants [85,97].

CPNs preparation

When developing a nanoparticle formulation, many variables account for the final characteristics of the product, for instance, mixing timescale [143], stirring speed [144], solvent [145], concentration of polymers and volume ratios of solvent and aqueous phase [146]. When considering light-absorbing organic macromolecules, the emission properties depend on structural features, such as the macromolecular arrangement and distribution of chromophores [8]. There is a complex relationship between molecular conformation and the optical and electrical properties of conjugated polymers [147,148]. For example, while fabrication conditions might not affect the size and shape of CPNs, it has been shown to have an impact on their spectroscopic properties [148]. In another example, the PEG-PLGA molecular weight influenced PCPDTBT photoacoustic properties, with low molecular weight PLGA (5 kDa) showing improved photoacoustic performance compared to 15 kDa or 55 kDa PLGA [136].

The optical properties of a conjugated polymer depend on the physical conformation of the polymer chains and, accordingly, they can vary between solution, films and compact nanoparticle structures [93,148–151]. In solution, the macromolecule conformation affects the extent of conjugation of a polymer and, accordingly, its optical properties [149]. For example, when the polymer chains are tightly coiled due to twisting of the polymer backbone, there is a shorter average conjugation length, leading to a blue shift in absorption and emission spectra [149,152,153]. In films and nanostructures, the conjugated polymers are restricted to a condensed architecture, which greatly increases the polymer chain contact [150], thus adjacent chromophores are packed more closely, facilitating their interaction and leading to the formation of inter-chain species that emit at longer wavelengths than the free polymer chain [149]. Overall, compared to fully solvated polymers in solvent, CPNs dispersed in water can present a blue-shifted absorption, related to the decreased conjugation length due to the polymer bending [86], and typically show a red-shift emission, caused by inter-chain species originating from increased chain interactions [9,86,92,93,132,142,148,154]. Importantly, the red-shifted emission is usually associated with a decrease in the quantum yield [86,132,142,148]. Therefore, it is important to consider the relationship between the conditions and materials used to prepare fluorescent nanoparticles with the properties and characteristics of the systems obtained.

The most common bulk methods for the preparation of polymeric nanoparticles are the mini-emulsion and the solvent displacement (also referred to as nanoprecipitation) techniques. The main difference between them is the polarity of the solvent used for the polymers [155]. In the nanoprecipitation method, a water-miscible solvent is used to dissolve the polymeric components, which is added in bolus, dropwise or by controlled addition to water (in the presence or absence of a surfactant) under stirring [155,156]. In contrast, the mini-emulsion technique uses a solvent not miscible in water to solubilise the polymers [155,156]. After the mixture of solvent solution and aqueous phase, the polymers assemble into nanoparticles and the solvent is removed by evaporation [144,156]. Both methods have been used extensively to synthesise CPNs [97,147,157–161].

Although nanoparticle size is a critical factor for biomedical applications, producing nanoparticles of a specific size range with good reproducibility is challenging and microfluidic-based CPN production techniques have been employed with reported success [134,162]. Besides the production of nanoparticles with tuneable size and low polydispersity, microfluidics systems are amenable to the high-volume production of CPNs [132] with the advantages of tuning their optical properties by controlling production conditions and generating high product yields [132]. The microfluidic production of CPN is typically based on the nanoprecipitation method [132,134,162].

Table 1: Chemical names and corresponding abbreviations of conjugated polymers and nanoparticle stabilising agents.

Abbreviation	Chemical name
Conjugated polymers	
PPV	Poly(p-phenylene vinylene) [16,87]
CPM-MDMO-PPV	Poly[2-(5'-methoxycarbonylpentyloxy)-5-methoxy-1,4-phenylenevinylene] (CPM-PPV-*co*-MDMOPPV) [97]
MEH-PPV	Poly[2-methoxy-5-(2-ethylhexyloxy)-1,4-phenylenevinylene] [20,87,88]
CN-PPV	Poly[2-methoxy-5-(2-ethylhexy-loxy)-1,4-(1-cyanovinylene-1,4-phenylene)] [92,137]; poly(2,5-di(hexyloxy)cyanoterephtalylidene) [135]
PPE	Poly(*p*-phenyleneethynylene) [15]

F8BT	Poly[(9,9-di-*n*-octylfluorenyl-2,7-diyl)-*alt*-(benzo[2,1,3]thiadiazol-4,8-diyl)] [138,139]
PFBT	Poly[9,9-dioctylfluorenyl-2,7-diyl)-*co*-4,7-benzo{2,1,3}-thiadiazole)] [93]
PFO	Poly (9,9-dioctylfluorenyl-2, 7-diyl) [99]
PFV	Poly[9,9-bis(2-(2-(2-methoxyethoxy)ethoxy)ethyl)fluorenyldivinylene-*alt*-9,9-bis(3-t-butylpropanoate)fluorene] [94]
PFBD	Poly[9,9-bis((6-N,N,N-trimethylammonium)hexyl)- fluorene-*alt*-*co*-(1,4-benzo-{2,10,3}-thiadiazole)] [6]; poly(9,9-dihexylfluorenyl-alt-2,1,3-benzooxadiazole) [98]; poly[9,9-bis((6-N,N,N-trimethylammonium)hexyl)fluorene-*alt*-*co*-2,1,3-benzoxadiazole dibromide] [133]
PFSBT	Poly[9,9-bis(40-sulfonatobutyl) fluorene-alt-co-(1,4-benzo- {2,10,3}-thiadiazole)] [6]
pDA	Poly(benzo[1,2-b:3,4-b']difuran-*alt*-fluorothieno-[3,4-b]thiophene) [91]
INDT	2,9-dihydroxy- 7,14-di(thiophen-2-yl)-diindolo[3,2,1-de:3',2',1'-ij][1,5]-naphthyridine-6,13-dione
PFTTQ	Poly[9,9-bis(4-(2-ethylhexyl)phenyl)fluorene-*alt*-*co*-6,7-bis(4-(hexyloxy)phenyl)-4,9-di(thiophen-2-yl)thiadi-azoloquinoxaline] [5]
PCPDTBT	Poly[2,6-(4,4-bis(2-ethylhexyl)-4H-cyclopenta-[2,1-b;3,4-b']dithiophene)-*alt*-4,7-(2,1,3-benzothiadiazole)] [3,18,19,62]
PIDT-DBT	Poly{[4,4,9,9-tetrakis(4-(octyloxy)phenyl-4,9-dihydro-s-indaceno[1,2- b :5,6- b ']dithiophene)]- *alt*-*co* -[4,7-di(thiophen- 2-yl)-2,1,3-benzothiadiazole]} [140]
PTD	Poly Poly[6-(2-ethylhexyl)-4-methyl-8-(5-methylthiophen-2-yl)-6,7-dihydro-5H-[1,2,3]triazolo[4',5':4,5]benzo[1,2-c][1,2,5]thiadiazole]-*alt*-[3-methyl-6-(5-methylthiophen-2-yl)-2,5-bis(2-octyldodecyl)-2,5-dihydropyrrolo[3,4-c]pyrrole-1,4-dione] Poly-thiadiazolobenzotriazole-*alt*-thiophene-diketopyrrolopyrrole [134]
PBTP-DPP	Poly((E)-3-(5-([8,8'-biindeno[2,1-b]thiophenylidene]-2-yl)thiophen-2-yl)-alt-2,5-bis(2-octyldodecyl)-6-(thiophen-2-yl)-pyrrolo[3,4-c]pyrrole-1,4(2H,5H)dione) [100]
PBMC	Poly[3-{2-[2,5-Bis-(2-ethyl-hexyloxy)-4-propenyl-phenyl]-vinyl}-9-butyl-6-methyl-9H-carba-zole]
Nanoparticle stabilising agents (surfactants/polymers/lipids)	
DSPE-PEG	1,2-distearoyl-*sn*-glycero-3-phosphoethanolamine-N-[methoxy(polyethyleneglycol)] [5,134,140]
DOPC	1,2-dioctanoyl-*sn*-glycero-3-phosphocholine [62]
DPPC	1,2-dipalmitoyl-*sn*-glycero-3-phosphocholine [3,88]
PEG	Polyethylene glycol [87]
PEG_{2000}-PE	1,2-diacyl-*sn*-glycero-3-phosphoethanolamine-N-(methoxy-(polyethylene glycol)-2000) [88]
PSMA	Poly(styrene-*co*-maleic anhydride) [17,92,137,141]
PLGA	Poly(lactide-*co*-glycolide) [94]
PEG-PLGA	Poly (ethylene glycol) methyl ether-*block*-poly (lactide-*co*-glycolide) copolymer
PEG-*b*-PPG-*b*-PEG	Triblock surfactant of PEG and poly-(propylene glycol) (PPG) [18]
PAAC*n*	poly(acrylate)s randomly substituted with hydrophobic linear alkyl groups [138]
lipid–Gd–DOTA	Gadolinium-1,4,7,10-tetraacetic acid modified phospholipid–PEG lipids [19]
BSA	Bovine serum albumin [100]
SDS	Sodium dodecylsulphate [97]

In vitro and *in vivo* applications of CPNs

For clarity, **Table 1** summarises the conjugated polymers and nanoparticle stabilising agents mentioned throughout the text. CPNs containing conjugated polymers with different optical properties in the visible and near infrared region of the spectra have been prepared with a range of coating agents and variable sizes for cell labelling and sensing applications (**Table 2**). For example, CPNs containing a type of cyano-substituted of PPV and the polymer PSMA with mean sizes of 16, 33 and 59 nm were internalised by the breast cancer cell line MCF-7 and when bioconjugated with streptavidin CPNs with the lowest size showed a more effective staining of cell membranes compared to their larger counterparts [92]. Moreover, magnetic MEH-PPV CPNs prepared with PEG_{2000}-PE/DPPC were visualised intracellularly in SH-SY5Y neuroblastoma cells, in spite of the large nanoparticle size distribution [88]. CN-PPV/PSMA CPNs conjugated with anti-σ-tubulin antibody enabled specific microtubule labelling of HeLa cells *in vitro* [137] (**Figure 4A**). Polymeric nanoparticles containing PFV and PLGA (>250 nm) were internalised by MCF-7 cells and cellular uptake was enhanced when the CPNs were functionalised with folic acid [94] (**Figure 4B**). In addition, PFV CPNs showed stable fluorescent signal after continuous laser excitation [94]. CPNs constituted solely of fluorene-tetraphenylethene conjugated polymers were able to encapsulate paclitaxel and showed a time dependent uptake and nuclei accumulation in human cervical (HeLa) and lung (A549) carcinoma cells [12], showing that CPNs can perform not only as staining agents but also as drug carriers [12]. Another study showed that biodegradable CPNs of PPE enabled selective mitochondria staining and presented greater cytocompatibility than the non-degradable counterpart in HeLa cells [15] (**Figure 4C**). The hydrophilic conjugated polymers PFBD and PFSBT generated CPNs of small sizes without the use of stabilising agents and were uptaken by SGC-7901 human gastric cancer cells [6]. In addition to bioimaging, PBMC CPNs stabilized with PSMA were used for *in vitro* Fe^{3+} biosensing in HeLa cells [17]. CPNs have also been engineered for photo-responsive drug release [16], in which an amphiphilic structure containing PPV functionalised with folic acid and a donor–acceptor Stenhouse adducts (DASA) promoted camptothecin and doxorubicin release *in vitro* following irradiation with a 550 nm laser for 60 min [16].

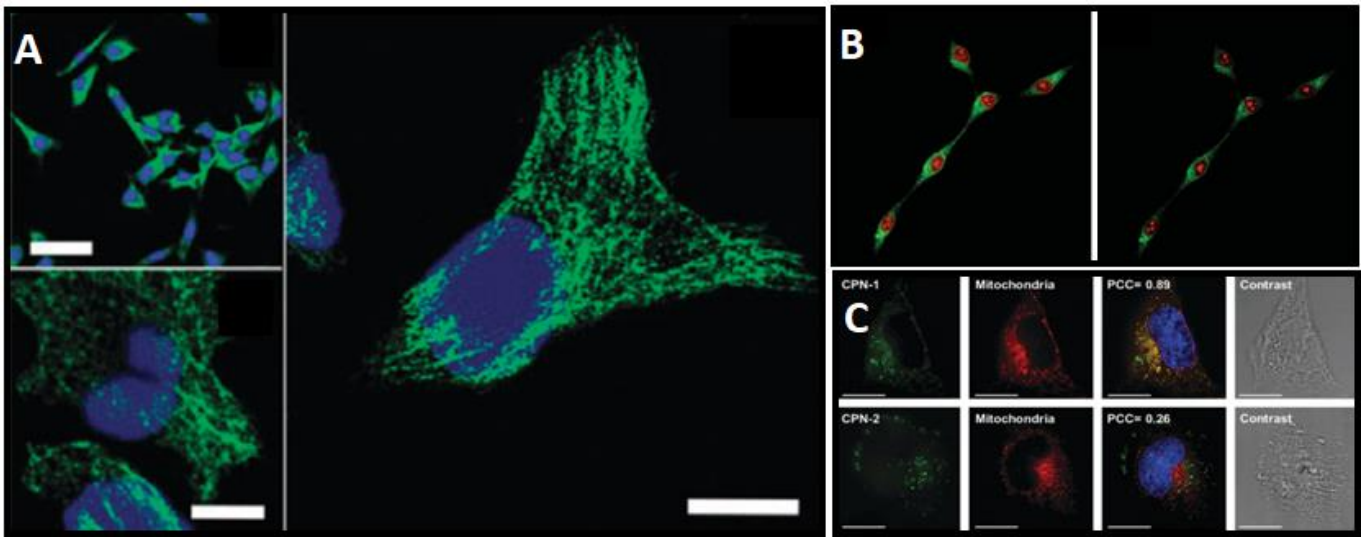

Figure 4: Microtubules imaging of HeLa cells following incubation with CN-PPV/PSMA CPNs bearing streptavidin and biotinylated anti-σ-tubulin (A). Bar represents 50 µm (A, top left) and 10 µm (A, bottom left and right). MCF7 cell uptake of PFV/PLGA CPNs functionalized with folate after 2.5h incubation, showing bright fluorescence (B left), which was stable after continuous laser illumination for 20 min (B right). PPE CPNs, which are biodegradable in the presence of glutathione, enabled mitochondria labelling of HeLa cells (top), while the non-degradable counterpart (bottom) showed nonspecific uptake following 18h incubation (C). Scale bar represents 20 µm (C). Reproduced from Ref. [137] Ye, F. *et al* (2012), Chemical Communications, 48(12), 1778–80 (A) and Ref. [15] Twomey, M. *et al* (2016), Chemical Communications, 52(27), 4910–13 (C) with permission from The Royal Society of Chemistry. Reproduced from Ref. [94] Li, B. K. *et al* (2009), Advanced Functional Materials, 19(22), 3535-42 (B), with permission from John Wiley and Sons.

For *in vivo* bioimaging, conjugated polymers with near infrared absorption have been studied as contrast agents. For example, near infrared cyano-substituted derivative of PPV stabilized with the surfactant Tween 80 enabled sentinel lymph node fluorescence mapping in mice after intradermal injection [85]. Moreover, CPNs containing pDA encapsulated in a PEGylated phospholipid shell with average size of < 6 nm, enabled rapid *in vivo* fluorescence imaging of blood flow in mice (**Table 2** and **Figure 5B**) [91]. Despite their lack of near infrared absorption, CPNs of MEH-PPV were investigated as a theranostic agent against TNBC [20] (**Figure 5A**). In this study, MEH-PPV encapsulated into DSPE-PEG_{2000} and functionalised with cyclic arginine-glycine-aspartic acid (cRGD) peptide was selectively taken up by $\alpha_v\beta_3$ integrin-overexpressed MDA-MB-231 TNBC cell line and induced cell death *in vitro*, both in 2D and 3D MDA-MB-231 models, after laser illumination [20]. The photo-responsive activity of the CPNs was attributed to ROS generation under laser illumination, which also inhibited the tumour growth in female BALB/c nude mice bearing MDA-MB-231 tumours and also showed greater accumulation in the tumour than in the mice liver and spleen [20].

Table 2: Polymer and stabilising agents used in CPNs, their size and applications, as reported in the literature.

Conjugated Polymer	CPN stabilising agent	Size (nm)	Application	Reference
Fluorene-tetraphenylethene based	Self-assembling conjugated polymer	70-90	Paclitaxel release and cell staining *in vitro* in HeLa and A549 cells	12
PFO	Polystyrene-PEG-COOH	20 ± 5.4	MCF7 cell staining *in vitro*	99
Polyfluorene based	Self-assembling conjugated polymer	~50	Mouse embryonic fibroblast cells and HCT116/PC12 3D spheroids staining and O_2 sensing *in vitro*	13
bis(diphenylaminostyryl)benzene-polyfluorene-dithienylbenzothiadiazole	PSMA	26	$HepG_2$ cell membrane staining *in vitro*	141
PPE	Self-assembling conjugated polymer	~140	Biodegradable conjugated polymers for targeted mitochondria imaging in HeLa cells	15

PFV	PLGA	258 ± 4	MCF-7 and NIH/3T3 cells staining *in vitro*	94
	PAAC*n*	<70	HEK 293 cells staining *in vitro*	138
F8BT	Transactivator (TAT) peptide	~40	HeLa cell staining *in vitro*	139
PFBD and PFSBT	Self-assembling hydrophilic conjugated polymer	<22	Fluorescent probes for human gastric cancer cells (SGC-7901) staining *in vitro*	6
	PEG_{300}	<20	HT-29 cell staining *in vitro*	98
PFBD	3-mercaptopropanoic acid functionalised with streptavidin	Not described	MCF-7 cell membrane staining *in vitro*	133
PFBT	PEG_{2000}-phospholipid	50	J774A.1 cell membrane staining *in vitro*	93
PPV	Self-assembling conjugated polymer	80	Photo-responsive CPNs for controlled drug release and imaging *in vitro* in HeLa cells	16
CPM-MDMO-PPV	SDS	117	C8-D1A, BV-2 and HMEC-1 cells staining	97
	PEG_{8000}	~100	CHO-K1 and h-TERT cells staining *in vitro*	87
MEH-PPV	PEG_{2000}-PE/DPPC	377 ± 266	SH-SY5Y cell staining *in vitro*	88
	$DSPE\text{-}PEG_{2000}$	36 ± 5	Triple negative breast cancer (TNBC) theranostic *in vivo*	20
	Hydrophobin (class I)	147 ± 50	HeLa cell staining *in vitro*	135
	PSMA	<59	MCF-7 cell staining *in vitro*	92
CN-PPV	Tween 80	60 ± 14	*In vivo* fluorescence imaging of sentinel lymph node	85
	PSMA	~12 nm	HeLa cell microtubules staining *in vitro*	137
PBMC	PSMA	~44	Fe^{3+} sensing *in vitro* in HeLa cells	17
	PEG-*b*-PPG-*b*-PEG	~50	*In vivo* photoacoustic and photothermal theranostic	18
	DOPC	59 ± 21	Fluorescence imaging and photothermal therapy i*n vitro* in HeLa cells	62
PCPDTBT	DPPC	~40	*In vivo* lymph node photoacoustic and fluorescence imaging	3
	PEG_{2000}-phospholipid	112 ± 3.2	*In vivo* photoacoustic multimodal imaging and photodynamic/photothermal therapy	19
	PSMA	<100	HCT-116 cell staining *in vitro*	142
PIDT-DBT	$DSPE\text{-}PEG_{2000}$	~56	*In vivo* imaging of liver tumor growth and *in vitro* cell tracing	140
INDT-BT	DPPC	160	*In vivo* photoacoustic vasculature imaging	4
PTD	DSPE-PEG	42	*In vivo* photoacoustic 3D vasculature imaging	134
PBTP-DPP	BSA	~11	*In vivo* photoacoustic imaging of mice breast cancer tumour	100
pDA	DSPE-mPEG (5 kDa)	< 6	*In vivo* fluorescence imaging of blood flow	91
PFTTQ	$DSPE\text{-}PEG_{2000}$	~52	*In vivo* photoacoustic imaging of mice bearing breast cancer tumour xenograft	5

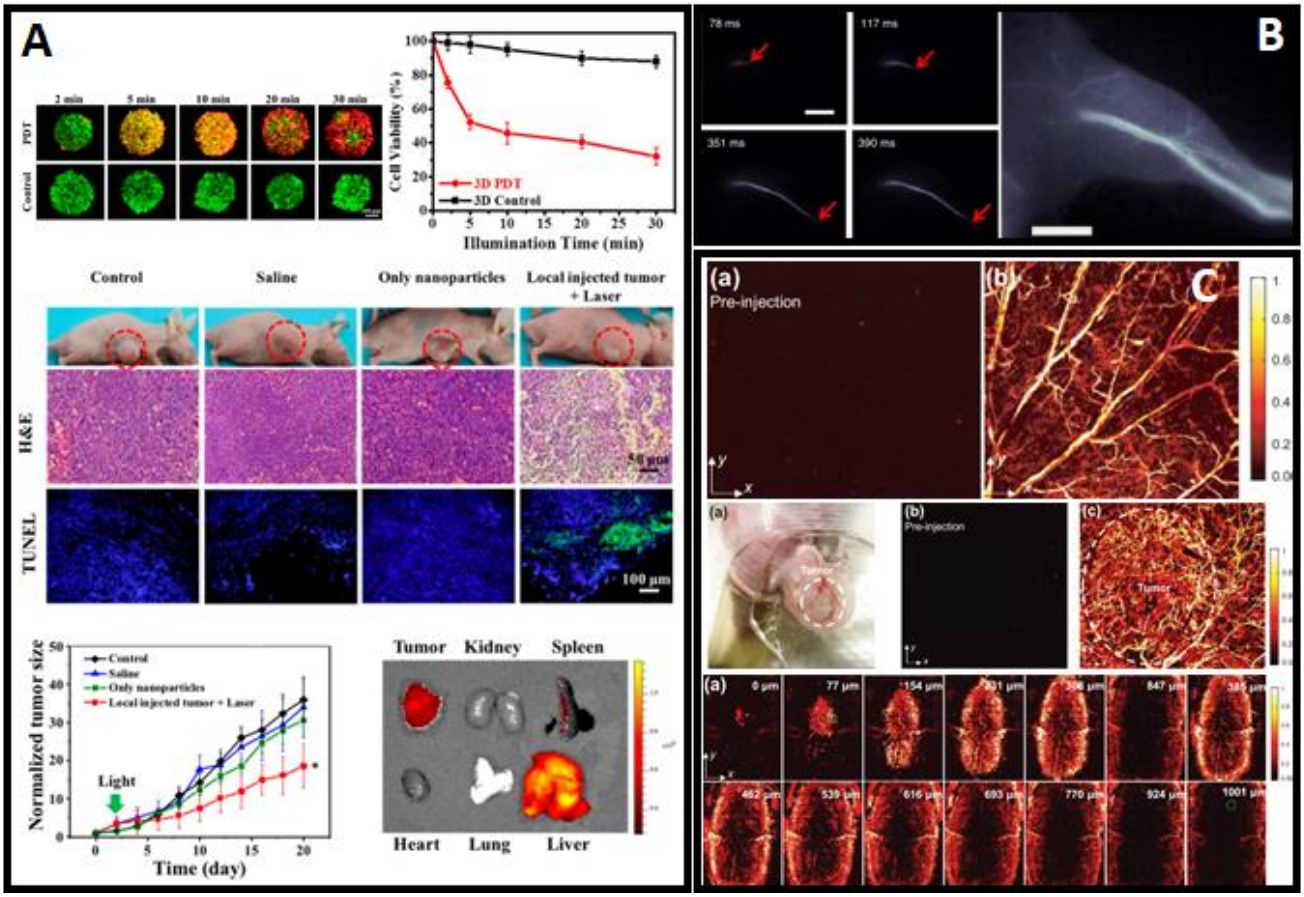

Figure 5: MDA-MB-231 3D spheroids incubated with MEH-PPV CPNs and exposed to white light irradiation for up to 30 min showed increased cell death visualised through the red fluorescent live/dead stain than the untreated cells (A top). MEH-PPV CPNs reduced the tumour growth 20 days after light irradiation and histology of tumour tissue revealed that it presented increased necrosis compared to the different treatments (A middle and bottom left images). *Ex vivo* images of mouse organs show high MEH-PPV CPNs accumulation in the tumour within 24h administration (A bottom right). Reprinted with permission from [20] Jin, G. et al (2018), ACS Applied Materials and Interfaces, 10(13), 10634-46 (A). Copyright (2018) American Chemical Society. CPNs of pDA showed fast fluorescence contrast of arterial blood flow after administration (B left images) and generated stable fluorescence imaging after the CPN perfusion through the mouse hindlimb (B right). Reprinted by permission from Springer Nature Customer Service Centre GmbH: Springer Nature, Nature Communications, Ultrafast fluorescence imaging *in vivo* with conjugated polymer fluorophores in the second near-infrared window, Hong, G. *et al* (2014) [91] (B). Photoacoustic contrast of the mouse ear vasculature after 5 min injection of PTD CPNs (C top). PTD CPNs also enabled the imaging of ear tumour vasculature (C middle) and through-skull brain vasculature visualisation (C bottom). Reproduced from Ref. [134] Guo, B. *et al* (2019) Advanced Materials, 31, 1-9 (C), with permission from John Wiley and Sons.

Conjugated polymers with near infrared absorption and emission have been explored not only for fluorescence imaging, but also as photoacoustic probes [3–5] and as photothermal agents for tumour ablation [18]. For example, PCPDTBT CPNs stabilised with DPCC showed strong photoacoustic and fluorescence signals in the lymph nodes after 24 hour injection in mice [3]. Importantly, the detection of photoacoustic emission of PCPDTBT/DPCC CPNs showed better image resolution and penetration depth than its fluorescence emission and they also enabled ROS detection *in vivo* when coupled with a ROS sensitive dye [3]. In addition, PCPDTBT CPNs prepared with PEG-*b*-PPG-*b*-PEG and doped with (6,6)-phenyl-C71-butyric acid methyl ester (PC70BM) provided photoacoustic contrast of the tumour after 6 hours administration and promoted tumour ablation following stimulation with a 808 nm laser for 5 minutes [18]. Lyu and collaborators [18] showed that the photoacoustic and photothermal performance of PCPDTBT was enhanced by incorporating an ultra-small carbon dot (PC70BM). Notably, PFTTQ CPNs functionalised with folate receptor had faster accumulation in mice bearing MCF7 xenografts than the untargeted ones, suggesting that targeted CPNs could achieve faster photoacoustic contrast than the ones subjected solely to passive EPR effect for tumour accumulation [5]. Photoacoustically active CPNs of INDT-BT stabilized with DPPC enhanced the visualisation of mouse vasculature *in vivo* in comparison to endogenous haemoglobin and deoxyhaemoglobin [4]. Similarly, CPNs of PTD encapsulated into DSPE-PEG_{2000} showed enhanced photoacoustic contrast for *in vivo* 3D vasculature imaging of the ear of heathy and tumour bearing mice, as well as of the animal brain vasculature (**Figure 4C**) [134]. CPNs have also been prepared with inorganic compounds to allow multimodal imaging, such as lipid micelles of PCPDTBT functionalised with gadolinium

used for photoacoustic and MRI imaging and photodynamic/photothermal therapy [19] and PBTP-DPP/gold CPNs stabilized with BSA prepared for photoacoustic and fluorescence imaging [100].

Generally, nanoparticles in the size range of *ca.* 15-260 nm were internalised or stained the cellular membrane of different cell lines, while for live imaging in mice, CPNs with sizes typically smaller than 150 nm have been studied as contrast agents. In regards to performance of the CPN material composition, while conjugated polymers have shown good cytocompatibility [12,15], CPNs stabilised with surfactants have been associated with increased cytotoxicity [87,131]. Notably, amphiphilic stabilising agents that show low toxicity and that can be processed and excreted following administration are preferable for *in vivo* applications. In this context, the nanoparticle safety assessment section below further highlights the importance of early biocompatibility screening of promising candidates.

Nanoparticle safety assessment

Despite the increasing presence of nanotechnologies in consumer goods, safety assessments and appropriate regulations concerning potential adverse effects on human health are still being developed at a much lower speed when compared with the availability of newly invented nanostructures [163,164]. Nonetheless, biocompatibility assays performed with standard techniques can provide relevant toxicological information and, accordingly, contribute to the understanding of the balance of harmful and beneficial effects as well as the establishment of safe exposition doses of nanoparticles [101,165]. While there has been concern regarding accidental exposure to nanomaterials, there is an enormous variety of nanoparticles specifically designed for biomedical applications. Their safety profile in living organisms, following intentional exposure, should be characterised according to current regulatory guidelines for medicines and medical products [164,166–169]. Among different techniques used for biocompatibility characterisation, *in vitro* assays are commonly used for preliminary safety assessments [101,166,167]. Although *in vitro* results cannot always be extrapolated to predict *in vivo* effects in humans, early toxicity screening of candidates can significantly improve the process of nanoparticle development by enhancing its efficiency and the probability of success [170,171].

Nanoparticles designed for biological sensing or cell labelling often have their biocompatibility investigated through *in vitro* cytotoxicity assays in desired cell types, according to the chosen application [87,94,167]. In contrast, delivery systems designed for *in vivo* applications are exposed to a much more complex environment and should perform their role without harming healthy tissues [101,166]. Nanoparticles can be administered via different routes with the objective of achieving accumulation in particular tissue areas or entire organs, although a large proportion of the administered dose will be distributed throughout the body and can interact with cells present in organs responsible for their clearance [105]. Nanoparticles can unintentionally interact with phagocytic cells, in particular with macrophages, which reside in various tissues [101,123,172] and are abundant in the liver and spleen where nanoparticles can accumulate following administration [105]. It is important to mention that targeted macrophage imaging also finds application for disease diagnosis in the presence of inflammatory processes [173] and, importantly, for understanding the role of tumour-associated macrophages in tumour progression [174]. Overall, preliminary safety assessments should ideally include the evaluation of potential toxic effects in cells present in tissues with targeted delivery, as well as with cells that might interact with nanoparticles following administration, such as phagocytic cells and blood components.

In an attempt to promote harmonized tests conditions, different organisations provide guidelines on recognised *in vitro* toxicity assays for nanoparticles [175], such as the American Society for Testing and Materials (ASTM), the International Organization for Standardization (ISO) and the Nanotechnology Characterization Laboratory (NCL), which offers standardized preclinical protocols. The protocols cover a large variety of relevant techniques, including aspects related the sample quality (e.g. nanoparticle physicochemical characterisation and the determination of product sterility and endotoxin content), which can greatly affect the product safety [169]. In particular, they describe various methods for *in vitro* biocompatibility assays, including cytotoxicity and haemocompatibility. There are numerous preclinical *in vitro* toxicity tests and the most common are described in **Table 3** [177–179].

Table 3: Summary of common preliminary *in vitro* biocompatibility assays for nanoparticles recognised by ISO/ASTM/NCL.

Characterisation	Parameter	Assay
Cell viability	Cellular membrane integrity	Trypan blue exclusion assay Lactate dehydrogenase (LDH)
	Cellular and lysosomal membrane integrity	Neutral red dye uptake
	Metabolic activity	Tetrazolium-based assays: - MTT ((3-(4, 5-dimethylthiazol-2- yl)-2, 5-diphenyltetrazolium bromide) - MTS (3-(4,5-dimethylthiazol-2-yl)-5-(3-carboxymethoxyphenyl)-2- (4-sulfophenyl)-2H-tetrazolium) -XTT ((2,3-bis(2-methoxy-4-nitro-5-sulfophenyl)-5-[(phenylamino) carbonyl]-2H-tetrazolium hydroxide))
Cytotoxicity	Vital stains	Flow cytometry
	Apoptosis	Caspase 3/7 activation

Phagocytic cell uptake	Macrophage interaction	Phagocytosis
Haemocompatibility	Red blood cell damage	Haemolysis
	Thrombogenicity	Platelet aggregation
	Rapid clearance and/or stimulatory release of proinflammatory factors	Complement system activation

Formulations designed for intravenous administration, should have their biocompatibility characterised with relevant blood components [101,166]. The most abundant cell type in the human peripheral whole blood is the red blood cells, followed by platelets and white blood cells [180]. Each one of these cell types has a vital role in the normal functioning of the body, with the red blood cells carrying gases involved in the respiration process [181], the platelets sealing wounds and preventing blood loss [182] and the white blood cells protecting the body against infections and exogenous materials [119,183]. Therefore, nanoparticles should ideally be inert to blood components. Haemolysis and platelet aggregation assays are recognised techniques to test the nanoparticle activity against these two cell types [131,166,178,184,185] and they can be performed with small volumes of blood freshly collected from volunteers.

In vitro cytotoxicity analyses are also broadly used to assess the biocompatibility of nanoparticles [167]. Assays based on cell culture have the advantages of reducing the need of animal experimentation and being less expensive and easier to control and reproduce [167,186]. Tissue culture *in vitro* involves the isolation of primary cells or the acquisition of cell lines and their culture in specialized vessels containing suitable cell culture medium (CCM) [177,187–190]. There are different cytotoxicity assays which can vary in their principles; some rely on the visual inspection of altered cellular morphology or differentiation of live/dead cells based on membrane permeability to specific dyes, while others are based on the evaluation of cellular metabolic functioning (**Table 3**).

While many reports of CPNs prepared for bioimaging applications have included cytotoxicity assessment in different cell lines [4,62,94,97,134,160,161,191–193], the study of the compatibility of CPNs with relevant blood components is less common in literature reports [131,134]. Additionally, many studies that have shown the potential applicability of CPNs as bioimaging agents did not include any biocompatibility assessment [9,85,91–93,95]. Although the physicochemical characterisation of CPNs is vital for the understanding of desired properties as imaging agents, a preliminary safety assessment provides important information about their biocompatibility and increases the chance of commercial/clinical applicability. In this context, an early safety assessment enables the screening of biocompatible CPNs components, as the material composition influences the properties in biological fluids and cell culture media. For example, previous works have reported that the type of surfactants used for nanoparticle assembly plays an important role in determining cellular uptake, biocompatibility and protein corona formation [161] and that PEGylated surfactants were prone to displacement by proteins after incubating the CPNs with serum and that the presence of unbound surfactant could cause increased haemolysis [131]. Additionally, excess of SDS surfactant in CPN solution was also related to increased cytotoxicity [87].

Conclusions

Conjugated polymers are versatile materials that have found many applications in the biomedical field. When assembled into nanoparticles, they have shown good performance as fluorescent contrast agents both *in vitro* and *in vivo* and as photoacoustic probes that be used both for diagnosis and cancer treatment. CPNs designed for biomedical applications have been formulated with different material composition and yielded nanoparticles of sizes typically below 250 nm. Common CPNs stabilising agents include lipids, polymers, proteins and surfactants, which could enable functionalisation with good targetability both *in vitro* and *in vivo*. The material composition and preparation technique can influence the physicochemical properties of CPNs, having great impact on their optical properties. In this context, the formulation of CPNs with regards to components and fabrication techniques plays an important role on their performance. Besides optimising their properties for biological applications, CPNs formulations also have an impact on their biocompatibility and an early safety screening with standardized techniques can enable a quicker transition of these promising materials to clinical/commercial applications. In this context, this review brings to light the role of CPNs within the bioimaging field, emphasizing important aspects of their formulation and safety assessment. The findings summarized and discussed here may contribute to the further development of CPNs and may be of interest for a wide audience interested in new materials with bioimaging applications.

Conflicts of interest

There are no conflicts to declare.

Acknowledgements

The Brazilian agency *Coordenação de Aperfeiçoamento de Pessoal de Nível Superior* (CAPES) and Science Without Borders programme for the full 4-year PhD scholarship and funding provided (process number 0685/13-5). We also acknowledge EPSRC for funding (EP/K018876/1).

Notes and references

1 J. Lin, B. Liu, M. Yu, X. Wang, Z. Lin, X. Zhang, C. Sun, J. Cabanillas-Gonzalez, L. Xie, F. Liu, C. Ou, L. Bai, Y. Han, M. Xu, W. Zhu, T. A. Smith, P. N. Stavrinou, D. D. C. Bradley and W. Huang, *Adv. Mater.*, 2019, **31**, 1–9.

2 K. M. Coakley and M. D. McGehee, *Chem. Mater.*, 2004, **16**,

4533–4542.

3 K. Pu, A. J. Shuhendler, J. V. Jokerst, J. Mei, S. S. Gambhir, Z. Bao and J. Rao, *Nat. Nanotechnol.*, 2014, **9**, 233–9.

4 T. Stahl, R. Bofinger, I. Lam, K. J. Fallon, P. Johnson, O. Ogunlade, V. Vassileva, R. B. Pedley, P. C. Beard, H. C. Hailes, H. Bronstein and A. B. Tabor, *Bioconjug. Chem.*, 2017, **28**, 1734–1740.

5 G. Balasundaram, C. J. H. Ho, K. Li, W. Driessen, U. S. Dinish, C. L. Wong, V. Ntziachristos, B. Liu and M. Olivo, *Int. J. Nanomedicine*, 2015, **10**, 387–397.

6 X. Guo, P. Li, Z. Liu, S. Yin, Z. Wang and Y. Wang, *J. Mater. Sci.*, 2017, **52**, 8465–8471.

7 A. J. Heeger, *Chem. Soc. Rev.*, 2010, **39**, 2354–71.

8 L. Akcelrud, *Prog. Polym. Sci.*, 2003, **28**, 875–962.

9 C. Wu, B. Bull, C. Szymanski, K. Christensen and J. McNeill, *ACS Nano*, 2008, **2**, 2415–2423.

10 K. Yu, B. Park, G. Kim, C. H. Kim, S. Park, J. Kim, S. Jung, S. Jeong, S. Kwon, H. Kang, J. Kim, M. H. Yoon and K. Lee, *Proc. Natl. Acad. Sci. U. S. A.*, 2016, **113**, 14261–14266.

11 D. Melling, J. G. Martinez and E. W. H. Jager, *Adv. Mater.*, 2019, **1808210**, 1–17.

12 Z. Wang, C. Wang, Y. Fang, H. Yuan, Y. Quan and Y. Cheng, *Polym. Chem.*, 2018, **9**, 3205–3214.

13 R. I. Dmitriev, S. M. Borisov, H. Düssmann, S. Sun, B. J. Müller, J. Prehn, V. P. Baklaushev, I. Klimant and D. B. Papkovsky, *ACS Nano*, 2015, **9**, 5275–5288.

14 T. Repenko, A. Rix, S. Ludwanowski, D. Go, F. Kiessling, W. Lederle and A. J. C. Kuehne, *Nat. Commun.*, 2017, **8**, 8–15.

15 M. Twomey, E. Mendez, R. K. Manian, S. Lee and J. H. Moon, *Chem. Commun.*, 2016, **52**, 4910–4913.

16 T. Senthilkumar, L. Zhou, Q. Gu, L. Liu, F. Lv and S. Wang, *Angew. Chemie - Int. Ed.*, 2018, **57**, 13114–13119.

17 Z. yan Gao, X. Zhang, S. Xing, Q. Lu, J. shui Yao, Q. ze Liu, C. de Qiao, R. xing Xie and B. Ding, *Dye. Pigment.*, 2019, **168**, 68–76.

18 Y. Lyu, Y. Fang, Q. Miao, X. Zhen, D. Ding and K. Pu, *ACS Nano*, 2016, **10**, 4472–4481.

19 D. Zhang, M. Wu, Y. Zeng, N. Liao, Z. Cai, G. Liu, X. Liu and J. Liu, *J. Mater. Chem. B*, 2016, **4**, 589–599.

20 G. Jin, R. He, Q. Liu, Y. Dong, M. Lin, W. Li and F. Xu, *ACS Appl. Mater. Interfaces*, 2018, **10**, 10634–10646.

21 T. F. Abelha, King's College London, 2018.

22 L. Fass, *Mol. Oncol.*, 2008, **2**, 115–152.

23 A. Aspect and P. Grangier, *Hyperfine Interact.*, 1987, **37**, 1–17.

24 J. A. Seibert, *J Nucl Med Technol*, 2004, **32**, 139–147.

25 M. Sauer, J. Hofkens and J. Enderlein, in *Handbook of Fluorescence Spectroscopy and Imaging*, WILEY-VCH Verlag GmbH & Co. KGaA, Weinheim, 2011, pp. 1–30.

26 J. M. Chadney, M. Galand, T. T. Koskinen, S. Miller, J. Sanz-Forcada, Y. C. Unruh and R. V. Yelle, *Astron. Astrophys.*, 2016, **587**, 1–14.

27 Z. Pachuau and R. C. Tiwari, *Sci. Vis.*, 2008, **8**, 128–136.

28 a Zamanian and C. Hardiman, *High Freq. Electron.*, 2005, **16**, 16–26.

29 B. H. Mahmoud, C. L. Hexsel, I. H. Hamzavi and H. W. Lim, *Photochem. Photobiol.*, 2008, **84**, 450–462.

30 P. Atkins and J. de Paula, *Physical Chemistry*, Oxford University Press, 8th edn., 2006.

31 P. Lang, K. Yeow, A. Nichols and A. Scheer, *Nat. Rev. Drug Discov.*, 2006, **5**, 343–356.

32 A. H. Fischer, K. A. Jacobson, J. Rose and R. Zeller, *Cold Spring Harb. Protoc.*, 2008, **3**, 3–5.

33 R. W. Burry, *J. Histochem. Cytochem.*, 2011, **59**, 6–12.

34 S. Kwon, C. H. Cho, Y. Kwon, E. S. Lee and J.-K. Park, *Sci. Rep.*, 2017, **7**, 1–10.

35 D. C. Peters, *J. Histochem. Cytochem.*, 1979, **27**, 241–245.

36 C. M. Pitsillides, J. M. Runnels, J. A. Spencer, L. Zhi, M. X. Wu and C. P. Lin, *Cytom. Part A*, 2011, **79 A**, 758–765.

37 R. P. Haugland, *Methods Cell Biol.*, 1994, **42**, 641–663.

38 M. Baker, *Nature*, 2011, **478**, 137–142.

39 J. C. Rasmussen, I. Tan, M. V Marshall, C. E. Fife and E. M. Sevick-Muraca, *Curr. Opin. Biotechnol.*, 2009, **20**, 74–82.

40 H. Lusic and M. W. Grinstaff, *Chem. Rev.*, 2013, **113**, 1641–1666.

41 S. S. Gambhir, *Nat. Rev. Cancer*, 2002, **2**, 683–693.

42 T. C. Lauenstein and R. C. Semelka, *Top. Magn. Reson. Imaging*, 2005, **16**, 15–20.

43 G.-P. Yan, L. Robinson and P. Hogg, *Radiography*, 2007, **13**, e5–e19.

44 A. Berger, *Br. Med. J.*, 2002, **324**, 35.

45 M. A. Schellpfeffer, *Birth Defects Res. Part C - Embryo Today Rev.*, 2013, **99**, 83–92.

46 I. Donald, J. MacVicar and T. G. Brown, *Lancet*, 1957, 1188–1195.

47 F. M. Abu-Zidan, A. F. Hefny and P. Corr, *J Emerg Trauma Shock*, 2011, **4**, 501–503.

48 F. Leblond, S. C. Davis, P. A. Valdés and B. W. Pogue, *J. Photochem. Photobiol. B Biol.*, 2010, **98**, 77–94.

49 Z. Guo, S. Park, J. Yoon and I. Shin, *Chem. Soc. Rev.*, 2014, **43**, 16–29.

50 M. Monici, in *Biotechnology Annual Review*, 2005, pp. 227–256.

51 L. Bachmann, *Appl. Spectrosc. Rev.*, 2006, **41**, 575–590.

52 C. Wu, J. Gleysteen, N. T. Teraphongphom, Y. Li and E. Rosenthal, *Int. J. Oral Sci.*, , DOI:10.1038/s41368-018-0011-4.

53 J. T. Senders, I. S. Muskens, R. Schnoor, A. V. Karhade, D. J. Cote, T. R. Smith and M. L. D. Broekman, *Acta Neurochir. (Wien).*, 2017, **159**, 151–167.

54 C. W. G. M. Löwik, E. Kaijzel, I. Que, A. Vahrmeijer, P. Kuppen, J. Mieog and C. Van de Velde, *Eur. J. Cancer*, 2009, **45**, 391–3.

55 X. Zhang, S. Bloch, W. Akers and S. Achilefu, *Curr. Protoc. Cytom.*, 2012, **60**, 1–28.

56 C. G. Hadjipanayis, H. Jiang, D. W. Roberts and L. Yang, *Semin. Oncol.*, 2011, **38**, 109–118.

57 M. Weiler, T. Kassis and J. B. Dixon, *J. Biomed. Opt.*, 2012, **17**, 066019-1-066019–11.

58 J. C. Rasmussen, I.-C. Tan, M. V Marshall, K. E. Adams, S. Kwon, C. E. Fife, E. a Maus, L. a Smith, K. R. Covington and E. M. Sevick-Muraca, *Transl. Oncol.*, 2010, **3**, 362–372.

59 E. M. Sevick-Muraca, S. Kwon and J. C. Rasmussen, *J. Clin. Invest.*, 2014, **124**, 905–914.

60 K. Li and B. Liu, *Chem. Soc. Rev.*, 2014, **43**, 6570–97.
61 R. R. Bouchard, O. Sahin and S. S. Emelianov, *IEEE Trans. Ultrason. Ferroelectr. Freq. Control*, 2014, **61**, 450–66.
62 J. Yoon, J. Kwag, T. J. Shin, J. J. Park, Y. M. Y. Lee, Y. M. Y. Lee, J. J. Park, J. Heo, C. Joo, T. J. Park, P. J. Yoo and S. Kim, *Adv. Mater.*, 2014, **26**, 4559–4564.
63 K. S. Valluru and J. K. Willmann, *Ultrason. (Seoul, Korea)*, 2016, **35**, 267–80.
64 A. P. Jathoul, J. Laufer, O. Ogunlade, B. Treeby, B. Cox, E. Zhang, P. Johnson, A. R. Pizzey, B. Philip, T. Marafioti, M. F. Lythgoe, R. B. Pedley, M. a. Pule and P. Beard, *Nat. Photonics*, 2015, **9**, 239–246.
65 A. G. Bell, *Am. J. Sci.*, 1880, **20**, 305–324.
66 A. Agarwal, S. W. Huang, M. O'Donnell, K. C. Day, M. Day, N. Kotov and S. Ashkenazi, *J. Appl. Phys.*, 2007, **102**, 064701–4.
67 A. De La Zerda, C. Zavaleta, S. Keren, S. Vaithilingam, S. Bodapati, Z. Liu, J. Levi, B. R. Smith, T.-J. Ma, O. Oralkan, Z. Cheng, X. Chen, H. Dai, B. T. Khuri-Yakub and S. S. Gambhir, *Nat. Nanotechnol.*, 2008, **3**, 557–562.
68 A. Becker, M. Masthoff, J. Claussen, S. J. Ford, W. Roll, M. Burg, P. J. Barth, W. Heindel, M. Schäfers, M. Eisenblätter and M. Wildgruber, *Eur. Radiol.*, 2018, **28**, 602–609.
69 L. V. Wang, *Med. Phys.*, 2008, **35**, 5758–5767.
70 Q. Fan, K. Cheng, Z. Yang, R. Zhang, M. Yang, X. Hu, X. Ma, L. Bu, X. Lu, X. Xiong, W. Huang, H. Zhao and Z. Cheng, *Adv. Mater.*, 2015, **27**, 843–847.
71 G. Hibbs, *Nat. Mater.*, 2014, **13**, 99–99.
72 A. M. Smith, H. Duan, A. M. Mohs and S. Nie, *Adv. Drug Deliv. Rev.*, 2008, **60**, 1226–1240.
73 B. Nordén and E. Krutmeijer, The Nobel Prize in Chemistry, 2000: Conductive polymers, http://www.nobelprize.org/nobel_prizes/chemistry/laureates/2000/advanced-chemistryprize2000.pdf.
74 C. K. Chiang, J. C. B. Fincher, Y. W. Park, A. J. Heeger, H. Shirakawa, E. J. Louis, S. C. Gau and A. G. MacDiarmid, *Phys. Rev. Lett.*, 1977, **39**, 1098–1101.
75 D. Braun, *Mater. Today*, 2002, 32–39.
76 J. H. Burroughes, D. D. C. Bradley, A. R. Brown, R. N. Marks, K. Mackay, R. H. Friend, P. L. Burns and A. B. Holmes†, *Nature*, 1990, **347**, 539–541.
77 P. S. Heeger and A. J. Heeger, *Proc. Natl. Acad. Sci. U. S. A.*, 1999, **96**, 12219–21.
78 L. Chen, D. W. McBranch, H. L. Wang, R. Helgeson, F. Wudl and D. G. Whitten, *Proc. Natl. Acad. Sci. U. S. A.*, 1999, **96**, 12287–92.
79 J. W. Blatchford, *Am. J. Phys.*, 1996, **64**, 120–135.
80 W. R. Salaneck, J. L. Friend and R. H. Bredas, *Phys. Rep.*, 1999, **319**, 231–251.
81 A. J. Heeger, *Angew. Chemie Int. Ed.*, 2001, **40**, 2591–2611.
82 Q. Pei, *Mater. Matters*, 2007, **2**, 26–30.
83 A. O. Patil, A. J. Heeger and F. Wudl, *Chem. Rev.*, 1988, **88**, 183–200.
84 D. R. Jones, B. Point and M. Levine, *J. Phys. Chem. B*, 2019, **123**, 4604–4610.
85 S. Kim, C.-K. Lim, J. Na, Y.-D. Lee, K. Kim, K. Choi, J. F. Leary and I. C. Kwon, *Chem. Commun.*, 2010, **46**, 1617–1619.
86 C. Wu, C. Szymanski and J. McNeill, *Langmuir*, 2006, **22**, 2956–60.
87 M. Green, P. Howes, C. Berry, O. Argyros and M. Thanou, *Proc. R. Soc. A*, 2009, **465**, 2751–2759.
88 P. Howes, M. Green, A. Bowers, D. Parker, G. Varma, M. Kallumadil, M. Hughes, A. Warley, A. Brain and R. Botnar, *J. Am. Chem. Soc.*, 2010, **132**, 9833–9842.
89 N. C. Greenham, I. D. W. Samuel, G. R. Hayes, R. T. Phillips, Y. A. R. R. Kessener, S. C. Moratti, A. B. Holmes and R. H. Friend, *Chem. Phys. Lett.*, 1995, **241**, 89–96.
90 M. Hanack, B. Behnisch, H. Häckl, P. Martinez-Ruiz and K.-H. Schweikart, *Thin Solid Films*, 2002, **417**, 26–31.
91 G. Hong, Y. Zou, A. L. Antaris, S. Diao, D. Wu, K. Cheng, X. Zhang, C. Chen, B. Liu, Y. He, J. Z. Wu, J. Yuan, B. Zhang, Z. Tao, C. Fukunaga and H. Dai, *Nat. Commun.*, 2014, **5**, 1–9.
92 K. Sun, H. Chen, L. Wang, S. Yin, H. Wang, G. Xu, D. Chen, X. Zhang, C. Wu and W. Qin, *ACS Appl. Mater. Interfaces*, 2014, **6**, 10802–10812.
93 P. K. Kandel, L. P. Fernando, P. C. Ackroyd and K. A. Christensen, *Nanoscale*, 2011, **3**, 1037–1045.
94 K. Li, J. Pan, S. S. Feng, A. W. Wu, K. Y. Pu, Y. Liu and B. Liu, *Adv. Funct. Mater.*, 2009, **19**, 3535–3542.
95 Y.-H. Chan, F. Ye, M. E. Gallina, X. Zhang, Y. Jin, I.-C. Wu and D. T. Chiu, *J. Am. Chem. Soc.*, 2012, **134**, 7309–12.
96 K. Li, Y. Liu, K. Y. Pu, S. S. Feng, R. Zhan and B. Liu, *Adv. Funct. Mater.*, 2011, **21**, 287–294.
97 M. Peters, N. Zaquen, L. D'Olieslaeger, H. Bové, D. Vanderzande, N. Hellings, T. Junkers and A. Ethirajan, *Biomacromolecules*, 2016, **17**, 2562–2571.
98 Y. Li, J. Liu, B. Liu and N. Tomczak, *Nanoscale*, 2012, **4**, 5694–5702.
99 A. Singh, M. Bezuidenhout, N. Walsh, J. Beirne, R. Felletti, S. Wang, K. T. Fitzgerald, W. M. Gallagher, P. Kiely and G. Redmond, *Nanotechnology*, 2016, **27**, 305603.
100 D. Gao, P. Zhang, Y. Liu, Z. Sheng, H. Chen and Z. Yuan, *Nanoscale*, 2018, **10**, 19742–19748.
101 S. Naahidi, M. Jafari, F. Edalat, K. Raymond, A. Khademhosseini and P. Chen, *J. Control. Release*, 2013, **166**, 182–194.
102 F. Klaessig, M. Marrapese and S. Abe, in *Nanostructure Science and Technology*, 2011, pp. 21–52.
103 H. Johnston, D. Brown, A. Kermanizadeh, E. Gubbins and V. Stone, *J. Control. release*, 2012, **164**, 307–13.
104 M. Auffan, J. Rose, J.-Y. Bottero, G. V. Lowry, J.-P. Jolivet and M. R. Wiesner, *Nat. Nanotechnol.*, 2009, **4**, 634–641.
105 M. C. Garnett and P. Kallinteri, *Occup. Med. (Lond).*, 2006, **56**, 307–11.
106 D. Ling, M. J. Hackett and T. Hyeon, *Nat. Mater.*, 2014, **13**, 122–124.
107 R. Dhankar, P. Rathee, A. K. Jain, S. Arora, S. Kumar, G. Rath, A. K. Saxena, P. R. Sharma and A. K. Goyal, *J. Appl. Pharm. Sci.*, 2011, **01**, 132–139.
108 M. E. Davis, Z. (Georgia) Chen and D. M. Shin, *Nat. Rev. Drug Discov.*, 2008, **7**, 771–782.
109 Y. Matsumura and H. Maeda, *Cancer Res.*, 1986, 6387–6392.
110 E. Blanco, H. Shen and M. Ferrari, *Nat. Biotechnol.*, 2015,

33, 941–951.
111 K. Zhang, X. Tang, J. Zhang, W. Lu, X. Lin, Y. Zhang, B. Tian, H. Yang and H. He, *J. Control. release*, 2014, **183**, 77–86.
112 S. K. Hobbs, W. L. Monsky, F. Yuan, W. G. Roberts, L. Griffith, V. P. Torchilin and R. K. Jain, *Proc. Natl. Acad. Sci. U. S. A.*, 1998, **95**, 4607–12.
113 F. Yuan, M. Dellian, D. Fukumura, M. Leunig, D. A. Berk, R. K. Jain and V. P. Torchilin, *Cancer Res.*, 1995, **55**, 3752–3756.
114 A. D. Wong, M. Ye, M. B. Ulmschneider and P. C. Searson, *PLoS One*, 2015, **10**, 1–13.
115 H. Maeda, *Adv. Enzyme Regul.*, 2001, **41**, 189–207.
116 H. Maeda, H. Nakamura and J. Fang, *Adv. Drug Deliv. Rev.*, 2013, **65**, 71–79.
117 J. I. Hare, T. Lammers, M. B. Ashford, S. Puri, G. Storm and S. T. Barry, *Adv. Drug Deliv. Rev.*, 2017, **108**, 25–38.
118 A. Kunzmann, B. Andersson, T. Thurnherr, H. Krug, A. Scheynius and B. Fadeel, *Biochim. Biophys. Acta*, 2011, **1810**, 361–73.
119 H. H. Gustafson, D. Holt-Casper, D. W. Grainger and H. Ghandehari, *Nano Today*, 2015, **10**, 487–510.
120 P. Del Pino, B. Pelaz, Q. Zhang, P. Maffre, G. U. Nienhaus, W. J. Parak, P. del Pino and P. D. U. Nienhaus, *Mater. Horizons*, 2014, **1**, 301–313.
121 M. Lundqvist, J. Stigler, G. Elia, I. Lynch, T. Cedervall and K. A. Dawson, *Proc. Natl. Acad. Sci. U. S. A.*, 2008, **105**, 14265–70.
122 F. Alexis, E. Pridgen, L. K. Molnar and O. C. Farokhzad, *Mol. Pharm.*, 2008, **5**, 505–515.
123 Y. Zhang, Y. Bai, J. Jia, N. Gao, Y. Li, R. Zhang, G. Jiang and B. Yan, *Chem. Soc. Rev.*, 2014, **43**, 3762–809.
124 H. Sarin, *J. Angiogenes. Res.*, 2010, **2**, 1–19.
125 F. Braet, E. Wisse, P. Bomans, P. Frederik, W. Geerts, A. Koster, L. Soon and S. Ringer, *Microsc. Res. Tech.*, 2007, **70**, 230–242.
126 H. S. Choi, W. Liu, P. Misra, E. Tanaka, J. P. Zimmer, B. Itty Ipe, M. G. Bawendi and J. V Frangioni, *Nat. Biotechnol.*, 2007, **25**, 1165–1170.
127 K. Li and B. Liu, *J. Mater. Chem.*, 2012, **22**, 1257–1264.
128 B. Romberg, W. E. Hennink and G. Storm, *Pharm. Res.*, 2008, **25**, 55–71.
129 F. M. Veronese and A. Mero, *BioDrugs Clin. Immunother. Biopharm. gene Ther.*, 2008, **22**, 315–29.
130 C. Y. Yu and A. S. Godana, *Eur. Polym. J.*, 2018, **99**, 165–171.
131 R. A. Khanbeigi, Z. Hashim, T. F. Abelha, S. Pitchford, H. Collins, M. Green and L. A. Dailey, *J. Mater. Chem. B*, 2015, **3**, 2463–2471.
132 T. F. Abelha, T. W. Phillips, J. H. Bannock, A. M. Nightingale, C. A. Dreiss, E. Kemal, L. Urbano, J. C. de Mello, M. A. Green and L. A. Dailey, *Nanoscale*, 2017, **9**, 2009–2019.
133 J. Liu, G. Feng, R. Liu, N. Tomczak, L. Ma, G. G. Gurzadyan and B. Liu, *Small*, 2014, **10**, 3110–3118.
134 B. Guo, J. Chen, N. Chen, E. Middha, S. Xu, Y. Pan, M. Wu, K. Li, C. Liu and B. Liu, *Adv. Mater.*, 2019, **31**, 1–9.
135 R. Peters, L. Sandiford, D. M. Owen, E. Kemal, S. Bourke, L. A. Dailey and M. Green, *Photochem. Photobiol. Sci.*, 2016, **15**, 1448–1452.
136 T. Abelha, P. R. Neumann, J. Holthof, C. A. Dreiss, C. Alexander, M. Green and L. A. Dailey, *J. Mater. Chem. B*, , DOI:10.1039/C9TB00937J.
137 F. Ye, C. Wu, Y. Jin, M. Wang, Y.-H. Chan, J. Yu, W. Sun, S. Hayden and D. T. Chiu, *Chem. Commun. (Camb).*, 2012, **48**, 1778–80.
138 L. Yan, X. Cui, T. Harada, S. F. Lincoln, S. Dai and T. W. Kee, *Macromolecules*, 2016, **49**, 8530–8539.
139 C. S. Almeida, I. K. Herrmann, P. D. Howes and M. M. Stevens, *Chem. Mater.*, 2015, **27**, 6879–6889.
140 J. Liu, K. Li and B. Liu, *Adv. Sci.*, 2015, **2**, n/a-n/a.
141 P. Liu, S. Li, Y. Jin, L. Qian, N. Gao, S. Q. Yao, F. Huang, Q. H. Xu and Y. Cao, *ACS Appl. Mater. Interfaces*, 2015, **7**, 6754–6763.
142 M. Fan, Y. Zhou, Y. Guo, J. Song and X. Duan, *Anal. Methods*, 2017, **9**, 3255–3259.
143 P. M. Valencia, O. C. Farokhzad, R. Karnik and R. Langer, *Nat. Nanotechnol.*, 2012, **7**, 623–9.
144 T. Kong, J. Wu, M. To, K. Wai Kwok Yeung, H. Cheung Shum and L. Wang, *Biomicrofluidics*, 2012, **6**, 34104.
145 P. Legrand, S. Lesieur, A. Bochot, R. Gref, W. Raatjes, G. Barratt and C. Vauthier, *Int. J. Pharm.*, 2007, **344**, 33–43.
146 S. Stainmesse, A.-M. Orecchioni, E. Nakache, F. Puisieux and H. Fessi, *Colloid. Polym. Sci.*, 1995, **273**, 505–511.
147 C. Szymanski, C. Wu, J. Hooper, M. A. Salazar, A. Perdomo, A. Dukes and J. McNeill, *J. Phys. Chem. B*, 2005, **109**, 8543–6.
148 H. Piwoński, T. Michinobu and S. Habuchi, *Nat. Commun.*, 2017, **8**, 15256.
149 B. J. Schwartz, *Annu. Rev. Phys. Chem.*, 2003, **54**, 141–172.
150 J. K. Grey, D. Y. Kim, B. C. Norris, W. L. Miller and P. F. Barbara, *J. Phys. Chem. B*, 2006, **110**, 25568–25572.
151 G. Padmanaban and S. Ramakrishnan, *J. Am. Chem. Soc.*, 2000, **122**, 2244–2251.
152 T.-Q. Nguyen, V. Doan and B. J. Schwartz, *J. Chem. Phys.*, 1999, **110**, 4068.
153 J. S. Kim, L. Lu, P. Sreearunothai, A. Seeley, K. H. Yim, A. Petrozza, C. E. Murphy, D. Beljonne, J. Cornil and R. H. Friend, *J. Am. Chem. Soc.*, 2008, **130**, 13120–13131.
154 G. Padmanaban and S. Ramakrishnan, *J. Phys. Chem. B*, 2004, **108**, 14933–14941.
155 C. E. Mora-Huertas, H. Fessi and a Elaissari, *Adv. Colloid Interface Sci.*, 2011, **163**, 90–122.
156 B. V. N. Nagavarma, H. K. S. Yadav, A. Ayaz, L. S. Vasudha and H. G. Shivakumar, *Asian J. Pharm. Clin. Res.*, 2012, **5**, 16–23.
157 S. Chambon, C. Schatz, V. Sébire, B. Pavageau, G. Wantz and L. Hirsch, *Mater. Horizons*, 2014, **1**, 431–438.
158 P. Howes and M. Green, *Photochem. Photobiol. Sci.*, 2010, **9**, 1159–1166.
159 P. Howes, M. Green, J. Levitt, K. Suhling and M. Hughes, *J. Am. Chem. Soc.*, 2010, **132**, 3989–3996.
160 E. Kemal, T. F. Abelha, L. Urbano, R. Peters, D. M. Owen, P. Howes, M. Green and L. A. Dailey, *RSC Adv.*, 2017, **7**, 15255–15264.
161 R. A. Khanbeigi, T. F. Abelha, A. Woods, O. Rastoin, R. D.

Harvey, M.-C. Jones, B. Forbes, M. A. Green, H. Collins and L. A. Dailey, *Biomacromolecules*, 2015, **16**, 733–742.
162 Z. Wang, B. Guo, E. Middha, Z. Huang, Q. Hu, Z. Fu and B. Liu, *ACS Appl. Mater. Interfaces*, 2019, **11**, 11167–11176.
163 F. Joris, B. B. Manshian, K. Peynshaert, S. C. De Smedt, K. Braeckmans and S. J. Soenen, *Chem. Soc. Rev.*, 2013, **42**, 8339–59.
164 I. Linkov, F. K. Satterstrom and L. M. Corey, *Nanomedicine nanotechnology, Biol. Med.*, 2008, **4**, 167–71.
165 G. Oberdörster, *J. Intern. Med.*, 2010, **267**, 89–105.
166 M. A. Dobrovolskaia, S. E. McNeil and S. E. M. Neil, *Nat. Nanotechnol.*, 2007, **2**, 469–78.
167 N. Lewinski, V. Colvin and R. Drezek, *Small*, 2008, **4**, 26–49.
168 H. Schellekens, S. Stegemann, V. Weinstein, J. S. B. De Vlieger, B. Flühmann, S. Mühlebach, R. Gaspar, V. P. Shah and D. J. A. Crommelin, *AAPS J.*, 2014, **16**, 15–21.
169 M. A. Dobrovolskaia, *J. Control. Release*, 2015, **220**, 571–583.
170 J. M. McKim, *Comb. Chem. High Throughput Screen.*, 2010, **13**, 188–206.
171 M. A. Dobrovolskaia and S. E. McNeil, *J. Control. Release*, 2013, **172**, 456–466.
172 C. A. Ruge, U. F. Schaefer, J. Herrmann, J. Kirch, O. Cañadas, M. Echaide, J. Pérez-Gil, C. Casals, R. Müller and C. M. Lehr, *PLoS One*, 2012, **7**, 1–10.
173 R. Weissleder, M. Nahrendorf and M. J. Pittet, *Nat. Mater.*, 2014, **13**, 125–38.
174 P. Pathria, T. L. Louis and J. A. Varner, *Trends Immunol.*, 2019, **40**, 310–327.
175 M. A. Dobrovolskaia, M. Shurin and A. A. Shvedova, *Toxicol. Appl. Pharmacol.*, 2016, **299**, 78–89.
176 NCL, Assay Cascade Protocols, https://ncl.cancer.gov/resources/assay-cascade-protocols, (accessed 15 September 2017).
177 C. F. Jones and D. W. Grainger, *Adv. Drug Deliv. Rev.*, 2009, **61**, 438–456.
178 M. a Dobrovolskaia, J. D. Clogston, B. W. Neun, J. B. Hall, K. Anil and S. E. Mcneil, *Nano Lett.*, 2009, **8**, 2180–2187.
179 J. M. Hillegass, A. Shukla, S. A. Lathrop, M. B. MacPherson, N. K. Fukagawa and B. T. Mossman, *Wiley Interdiscip. Rev. Nanomedicine Nanobiotechnology*, 2010, **2**, 219–231.
180 D. P. Cistola and M. D. Robinson, *TrAC Trends Anal. Chem.*, 2016, **83**, 53–64.
181 O. S. Hajjawi, *Am. J. Life Sci.*, 2013, **1**, 195–214.
182 R. Paniccia, R. Priora, A. A. Liotta and R. Abbate, *Vasc. Health Risk Manag.*, 2015, **11**, 133–148.
183 Y.-K. Chan, M.-H. Tsai, D.-C. Huang, Z.-H. Zheng and K.-D. Hung, *BMC Bioinformatics*, 2010, **11**, 2–18.
184 ASTM F 756-00, *Standard practice for assessment of hemolytic properties of materials.*, 2000.
185 M. a Dobrovolskaia, P. Aggarwal, J. B. Hall and S. E. Mcneil, *Mol. Pharm.*, 2009, **5**, 487–495.
186 M. A. Elsheikh, Y. S. R. Elnaggar and O. Y. Abdallah, *J. Control. Release*, 2014, **194**, 92–102.
187 J. R. Masters and G. N. Stacey, *Nat. Protoc.*, 2007, **2**, 2276–2284.
188 B. Kong, J. H. Seog, L. M. Graham and S. B. Lee, *Nanomedicine*, 2011, **6**, 929–941.
189 W. I. Schaeffer, *In Vitro*, 1984, **20**, 19–24.
190 J. R. Masters, *Nat. Rev. Mol. Cell Biol.*, 2000, **1**, 233–236.
191 H. Zhu, Y. Fang, X. Zhen, N. Wei, Y. Gao, K. Q. Luo, C. Xu, H. Duan, D. Ding, P. Chen and K. Pu, *Chem. Sci.*, 2016, **7**, 5118–5125.
192 X. Zhen, X. Feng, C. Xie, Y. Zheng and K. Pu, *Biomaterials*, 2017, **127**, 97–106.
193 C. M. Macneill, R. C. Coffin, D. L. Carroll and N. H. Levi-Polyachenko, *Macromol. Biosci.*, 2013, **13**, 28–34.